NIH Public Access
Author Manuscript
J Vasc Interv Radiol. Author manuscript; available in PMC 2009 September 21.

Published in final edited form as:
J Vasc Interv Radiol. 2008 October ; 19(10): 1490–1496. doi:10.1016/j.jvir.2008.06.008.

Distribution of Iron Oxide–containing Embosphere Particles after Transcatheter Arterial Embolization in an Animal Model of Liver Cancer: Evaluation with MR Imaging and Implication for Therapy

Kwang-Hun Lee, MD, **Eleni Liapi, MD**, **Josephina A. Vossen, MD**, **Manon Buijs, MD**, **Veronica Prieto Ventura, MD**, **Christos Georgiades, MD, PhD**, **Kelvin Hong, MD**, **Ihab Kamel, MD**, **Michael S. Torbenson, MD**, and **Jean-Francois H. Geschwind, MD**
From the Division of Vascular and Interventional Radiology, The Russell H. Morgan Department of Radiology and Radiological Science (K.H.L., E.L., J.A.V., M.B., V.P.V., C.G., K.H., I.H., J.F.H.G.), and Department of Pathology (M.S.T.), The Johns Hopkins University School of Medicine, 600 North Wolfe Street, Blalock 545, Baltimore, MD 21287; and Division of Interventional Radiology, Department of Radiology and Research Institute of Radiological Science (K.H.L.), Severance Hospital, Yonsei University College of Medicine, Seoul, Republic of Korea.

Abstract

PURPOSE—To test whether different-sized iron oxide– containing Embosphere (IOE) particles can be detected by dedicated magnetic resonance (MR) imaging when injected intraarterially in an animal model of liver cancer and whether their distribution could be accurately predicted by MR imaging before confirmation with histopathologic analysis.

MATERIALS AND METHODS—Twenty New Zealand White rabbits implanted with VX2 liver tumor were randomly assigned to undergo embolization with 100 –300-μm particles (group S; n = 10) or 300 –500-μm particles (group L; n = 10). Embolization was performed with the catheter placed in the proper hepatic artery. T2*-weighted multiplanar MR imaging was performed within 24 hours after the procedure to detect paramagnetic IOE susceptibility artifact. MR imaging interpretation parameters included presence of artifact in the artery and/or at the tumor bed. Hematoxylin and eosin– and Prussian blue–stained pathologic slides were also obtained and the presence of IOE was evaluated similarly.

RESULTS—The MR detectability rates for IOEs were 100% in both groups. Paramagnetic susceptibility IOE artifact inside the tumor was detected in 30% of group S animals. On pathologic analysis, IOE particles were detected inside the tumor in 70% of this group. IOEs in group L were found outside the tumor within the hepatic artery on MR imaging and histopathologic study (P < . 05).

CONCLUSIONS—MR imaging readily detected IOE particles in an animal model of liver cancer regardless of the particle size. The smaller particles (100 –300 μm) were delivered inside the tumor or in close proximity to the tumor margin, justifying their use for drug delivery or precise embolization.

Embolization of liver tumors, in the form of bland embolization, transcatheter arterial chemoembolization, or radioembolization with yttrium-90, is one of the most commonly

© SIR, 2008

Address correspondence to J.F.H.G.; jfg@jhmi.edu.

From the SIR 2008 Annual Meeting.

None of the other authors have identified a conflict of interest.

NIH-PA Author Manuscript
NIH-PA Author Manuscript
NIH-PA Author Manuscript

NIH-PA Author Manuscript

NIH-PA Author Manuscript

NIH-PA Author Manuscript

performed interventional radiologic procedures for the treatment of patients with primary or secondary liver cancer (1–4). Various embolic devices with different morphologic, chemical, and physiomechanical properties are currently employed during these procedures (3) . Among the most commonly used embolic devices are microspheres, which can be made of resorbable or nonresorbable materials, easily calibrated and accurately graded, or effectively drug-loaded and copolymerized with other biocompatible compounds (5–10).

Magnetic resonance (MR) imaging is attractive as an imaging technique because it combines the benefits of high spatial resolution with physiologic information on a specific area. The introduction of iron as an integral component of microspheres is appealing because the presence of ferromagnetic material within tissue can be easily detected on MR imaging (11–13). Until the present time, iron-loaded embolic microspheres have been mainly used with the concurrent application of an external alternating magnetic field as a combination of hyperthermia treatment and permanent vessel occlusion (14).

Tris-acryl gelatin microspheres (Embosphere Microspheres; Biosphere Medical, Rockland, Massachusetts) are calibrated, hydrophilic, nonresorbable biocompatible embolic microspheres that are routinely used during liver embolization procedures (3). The choice of Embosphere size for liver embolization procedures often depends on the operator′s preference, as there have been no solid data advocating the use of one size versus another (3). Moreover, delineation of their preferential distribution in the tumor bed has been limited to a few studies that used invasive or experimental methods (15–17). Therefore, the development of a new class of embolic microspheres detectable by imaging—and a reliable noninvasive imaging method capable of identifying the distribution of these microspheres in tumor and nontumorous tissue—may be of significance when choosing the most appropriate particle size for embolization or drug delivery.

In this study, we used two different sizes of iron oxide–loaded Embospheres for transcatheter arterial embolization of the VX2 liver tumor model and subsequently evaluated their distribution in liver tissue by dedicated MR imaging and histopathologic analysis. We aimed to assess the feasibility of using such microspheres for liver embolization procedures, evaluate their detectability by MR imaging, and identify a pattern of preferential distribution according to microsphere size.

MATERIALS AND METHODS

Study Design

Our institution′s animal care and use committee approved the study, and all animal care and use procedures were performed under our institutional guidelines. A total of 24 adult New Zealand White male rabbits (Myrtle′s Rabbitry, Thompson Station, Tennessee) weighing 3.8–4.3 kg were used for this study. Four rabbits were used as tumor carriers for the study rabbits and 20 study rabbits underwent implantation in the liver with VX2 tumor before undergoing embolization. These study rabbits were then randomly assigned to two groups of 10 animals each (groups S and L): group S animals received intraarterial hepatic embolization with iron oxide–containing Embosphere (IOE) microspheres measuring 100–300 μm in size, whereas group L animals were treated with IOEs measuring 300–500 μm in size. All animals underwent imaging in a 1.5-T clinical MR imaging scanner within 24 hours after embolization with a dedicated iron-detecting protocol. All animals were subsequently euthanized after scanning, and liver and tumor sections were sent for histopathologic analysis of IOE detection and distribution.

NIH-PA Author Manuscript

NIH-PA Author Manuscript

NIH-PA Author Manuscript

Animal Tumor Implantation

Anesthesia was induced with an intramuscular injection of acepromazine (2.5 mg/kg; Phoenix, St. Joseph, Missouri) and ketamine (44 mg/kg; Phoenix) and maintained via a marginal ear vein with sodium pentobarbital (2.5–5 mg; Abbott Laboratories, North Chicago, Illinois) during all animal interventions. VX2 tumor cell suspensions were prepared and provided by J. Hilton, MD. Each rabbit tumor carrier received a single intramuscular injection of 125 μL of VX2 tumor cell suspensions on each hind leg. After 12–14 days, the intramuscularly grown tumors were harvested and preserved in normal saline solution until completion of the implantation procedures, and the carriers were euthanized with slow intravenous injection of pentobarbital. All VX2 liver tumor implantation procedures were carried out in a sterile fashion. The liver of each rabbit was exposed with a midline subxiphoid incision, and a single small tumor piece (approximately 3 mm^3) was implanted directly into the left lateral lobe of the liver. Manual compression over the point of tumor insertion was then applied for 30 seconds, followed by surgical closure of the abdomen in two layers. The tumors were allowed to grow in the rabbit livers for 13–15 days, after which time a well demarcated solitary tumor was expected to grow to a size of 1.5–2.0 cm in diameter (18,19). After surgery, the animals were placed in cages and monitored until they fully recovered from anesthesia.

Preparation of Embolization Material

Iron oxide–containing tris-acryl gelatin microspheres (Biosphere Medical, Rockland, Massachusetts) were synthesized with use of an emulsion polymerization process involving tris-acryl monomer and iron oxide nanoparticles. The iron oxide was introduced in the monomer phase before the polymerization phase. Microspheres were then washed several times with water and passed through a sieve to isolate several size ranges: 100–300 μm, 300–500 μm, 500–700 μm and 700–900 μm. The samples were tested at dosages with isomolar iron content. The iron concentration was optimized in a previous report and standardized at 670 mg Fe/L (20).

In Vitro MR Imaging

Microspheres from the different size ranges were mixed and dispersed with trypcase soja gel. The mixture was introduced in glass tubes for imaging evaluation by employing low-resolution MR imaging (1.5 T, T1 spinecho sequence).

Embolization Materials for Animal Studies

IOE microspheres were provided by the manufacturer in vials of 100 – 300 μm and 300 –500 μm maximum diameters, which were used for all embolization procedures. A total of 5 mL of particles was diluted in 15 mL of 0.9% sodium chloride and 10 mL contrast medium (Omnipaque; Amersham, Piscataway, New Jersey), making the total volume of IOE suspension 30 mL.

Transcatheter Hepatic Arterial Embolization Technique

All rabbits were anesthetized and intubated, and their CO_2 was monitored throughout the procedure. Access into the right common femoral artery was obtained via a surgical cut-down, after which a 3-F sheath (Cook, Bloomington, Indiana) was inserted. A 2-F JB1 catheter (Cook) was then manipulated into the common hepatic artery and arteriography was performed to delineate the hepatic arterial anatomy and tumor staining (Fig 1). After adequate catheter positioning was achieved at the level of the proper hepatic artery, the IOE suspension was slowly administered under fluoroscopic guidance. The endpoint of the embolization procedure was lobar arterial inflow reduction with concurrent maintenance of proper hepatic arterial inflow. After the procedure, the common femoral artery was ligated with absorbable sutures.

NIH-PA Author Manuscript

NIH-PA Author Manuscript

NIH-PA Author Manuscript

MR Imaging Protocol and Analysis

All animals underwent imaging within 24 hours after embolization with IOE. Baseline MR imaging was performed before embolization in five animals. All animals were anesthetized and intubated before imaging. MR imaging was performed at 1.5 T (Signa; General Electric Medical Systems, Milwaukee, Wisconsin). Each animal was placed inside an extremity coil and covered with a blanket. Imaging protocol consisted of T2-weighted fast spin-echo images (matrix size, 128 × 128; slice thickness, 5 mm; interslice gap, 5 mm; repetition/echo times, 1,800/78.62 msec; receive bandwidth, 32 kHz), T1-weighted two-dimensional fat-suppressed spoiled gradient-echo images (field of view, 16 × 16; matrix, 512 × 192; slice thickness, 5 mm; repetition/echo times, 150/2.088 msec; receive bandwidth, 64 kHz; flip angle, 15°), and T2*-weighted multi-planar images (field of view, 16 × 16; matrix size, 256 × 160; repetition/echo times, 200/15 msec; flip angle, 45°; slice thickness, 5 mm; interslice gap, 5 mm).

Images were evaluated by consensus of two experienced MR imaging radiologists who were unaware of the histopathologic findings. Qualitative MR imaging interpretation was based on T2*-weighted images, assuming that the IOEs produce a strong signal reduction artifact in this sequence. In each T2*-weighted study, the presence or absence of signal voids was first recorded. In case of present signal decays, the IOE distribution was further described in relation to two anatomic structures and based on a subjective two-tier scale: (i) artifact in the artery and (i) artifact in the tumor bed (at the periphery of the tumor or inside the tumor). The presence of an artifact related to the tumor was further subjectively scored as 1, 2, or both, with 1 indicating artifact in the artery and 2 indicating artifact in the tumor bed at the periphery or inside the tumor.

Histopathology

Within 1–2 hours after completion of MR imaging, all animals were euthanized under deep anesthesia by slow intravenous injection of sodium pentobarbital. All livers were then explanted and preserved in 10% formaldehyde for at least 4 days, after which time gross liver tumor specimens were cut in 5-mm sections and labeled according to the MR imaging anatomic orientation. Each section was then embedded in paraffin, and four slices (approximately 4 μm each) from each section were stained with hematoxylin and eosin and Perls Prussian blue.

All slides were reviewed by an independent pathologist for detection and localization of the IOE. In each slide, the presence or absence of microspheres was first recorded. In case of present microspheres, a more detailed evaluation was then performed. Their presence was scored on a scale similar to the MR scoring scale, with a score of 1 indicating IOE particles in an artery and a score of 2 indicating IOE particles in the tumor bed at the periphery of the tumor or inside the tumor.

Statistics

All data were analyzed with the statistical package STATA (version 9; Stata, College Station, Texas). Statistical analysis included *t* tests, Wilcoxon rank tests, and Pearson correlation analysis for all tested parameters. Differences were considered statistically significant at *P* values less than .05.

RESULTS

Liver tumor growth was successful in both animal groups, with a consistent mean maximum tumor diameter of 1.65 cm ± 0.33 (SD), as measured on axial T1-weighted MR images. All rabbits underwent successful intraarterial embolization. No technical difficulties or periprocedural complications were observed. A prominent tumor-feeding artery arising off the left hepatic artery was identified in all cases. In group S, 10 mL of the total 30 mL of IOE

NIH-PA Author Manuscript

NIH-PA Author Manuscript

NIH-PA Author Manuscript

suspension was successfully injected according to the endpoint of the embolization procedure, whereas in group L, 5 mL of the of total 30 mL of IOE solution was injected. This was a result of the size difference in IOEs used between groups.

The VX2 tumors were identified as spherical or ovoid solid structures within the left hepatic lobe, with low signal intensity on T1-weighted images, high signal intensity on T2-weighted images, and relatively high signal intensity on T2*-weighted images. All preembolization baseline MR imaging performed in five rabbits demonstrated homogenous high signal intensity, and there were no dark signal intensity spots that could possibly cause false-positive findings when evaluating the postembolization MR imaging.

After embolization with IOEs, distinctive signal voids representing clusters of IOEs could be identified in the liver (right and left lobes and gallbladder) and/or in the tumor area. Quantification of IOE distribution according to size is shown in the Table. T2*-weighted MR imaging was 100% sensitive in both groups in the detection of signal decay caused by the IOEs. A signal void in tumor feeding arteries was detected in all cases in both groups. In group S, the signal void was identified circumferentially around the tumor in all cases and inside the tumor in 30% of cases (Fig 2). None of the animals in group L showed similar signal decay inside the tumor ($P = .004$), but rather, signal dropoff was found partially distributed at the periphery of the tumor and at a distance from the tumor within the hepatic artery (Fig 3). Quantification of the artifact revealed a significantly higher score in group S than in group L (20 vs 16; $P < .05$).

On histopathologic analysis, IOE particles were identified as bright pink spheres on hematoxylin and eosin–stained specimens and were translucent with a green rim on Perls Prussian blue–stained specimens. IOEs were detected inside the tumor in 70% of all group S animals (Fig 4). Conversely, intratumoral IOE deposition was not detected in any of the group L animals ($P < .05$), confirming the MR imaging findings.

There was no significant difference between groups regarding MR artifact in the artery and the histopathologic presence of particles in the artery ($P > .9999$). However, there was significant difference when comparing the MR artifact ($P = .0368$) and the histopathologic presence of particles ($P = .0051$) in the tumor bed between the two groups. There was positive MR imaging and histopathologic correlation in both groups (Pearson $\rho = .667$; $P = .0332$) for the distribution of IOEs in the tumor bed.

DISCUSSION

Several embolic agents have been employed during the past two decades to maximize the effects of transcatheter intraarterial therapy for hepatic malignancies (3,19). The level of their vascular and peri-and intratumoral distribution has been selectively confirmed, mostly by invasive histopathologic analysis (21,22). Therefore, the fabrication of microspheres that can be noninvasively detected holds great promise for further refinement of the embolization technique, as well as determination of particle size for drug delivery. Our study introduces iron oxide–loaded tris-acryl gelatin microspheres for hepatic embolization procedures, which can be easily detected and tracked noninvasively by dedicated MR imaging. By tracking the delivery of these microspheres, such an MR imaging protocol, which is already used clinically, could provide valuable information on the differences in distribution of these microspheres based on their size. The results of our study are significant because we showed that IOEs could indeed be imaged and tracked by MR imaging and that the distribution of these microspheres within the tumor (or outside the tumor for the larger beads) could have major clinical implications.

NIH-PA Author Manuscript

NIH-PA Author Manuscript

NIH-PA Author Manuscript

Two key points should be addressed that have helped us achieve the results described. First, we diluted the vial of IOE and injected the IOE suspension slowly in accordance with arterial pulsatility into the tumor-feeding artery. The dilution of the IOE suspension and the slow pulsatile injection rate not only prevent spasmodic change of the feeding artery that would limit the amount of embolic agent delivered, they also enable the solution to flow along the bloodstream toward the tumor bed. As the main feeding artery gradually fills with IOEs, the flow kinetics decrease and the IOEs travel at a slower speed until they gradually saturate the feeding vessels. It has been shown that bolus injection of microspheres may lead to particle congregation and congestion at a more proximal site of the feeding branches (22). Therefore, it seems that the embolization technique may be initially modified by adapting the volume, dilution, and injection rate of microspheres.

Second, IOEs are ferromagnetic particles, which tend to agglomerate because of their permanent magnetic dipoles. One would assume that it could be difficult to achieve successful targeting without an external magnetic field. However, dilution to decrease the density in the injected volume and the slow pulsatile injection rate, assisted by the vessel′s normal blood flow, appeared to overcome the microspheres′ intrinsic magnetic forces. In our study, microsphere agglomeration was sufficient to cause a distinctive signal void on T2*-weighted MR imaging without compromising their mobility.

T2*-weighted MR imaging is routinely used to depict the presence of iron in the hepatic parenchyma. However, the paramagnetic signal intensity on T2*-weighted imaging has been shown to depend on microsphere size and the degree of microsphere aggregation. Moreover, this paramagnetic effect is influenced by the strength of the magnetic field, the magnetic property of the core, and echo time (11,23). In our study, there was positive MR imaging and histopathologic correlation in both groups for the distribution of IOEs in the tumor bed. However, MR imaging was weaker in demonstrating the presence of IOEs in group S compared with pathologic analysis. One could attribute this discrepancy to (i) the low signal-to-noise ratio of these microspheres when lodged inside the tumor, (ii) their size, or (iii) the low aggregation effect caused by individual trapping of smaller microspheres inside the tumor vessels. Individually trapped, isolated IOEs may be hard to detect on MR imaging as a result of low signal-to-noise ratio of a single small particle or slice misregistration. Further studies should be performed to confirm these assumptions.

In the present study, we clearly demonstrated that small Embospheres lodged inside the tumor (including the rim of the tumor), whereas their larger counterparts remained outside the tumor. Nevertheless, the optimal sphere size for any given hepatic tumor remains to be determined. This might be difficult to assess only by estimating vessel size, observing the slowing of arterial flow, or depicting deeper penetration of smaller IOEs into the abnormal tumor vascular bed. Further studies should be performed to accurately correlate microsphere size, level of arterial obstruction, and tumoricidal effect. Nonetheless, we can state that, if the purpose of embolization is to deliver microspheres as close to the tumor as possible or even within the tumor bed, the small particles measuring 100–300 μm should be used. In this regard, our finding may have some important implications for new drug delivery systems. Again, knowing that drugs cannot travel long distances within the tumor microenvironment, it is essential and highly desirable to deliver them as close to the tumor as possible. A single previous report (22) demonstrated that the level of vascular occlusion with calibrated tris-acryl microspheres precisely correlated with particle size. We could therefore infer from that report that 100-μm particles should occlude vessels of matching size. Yet, it is important to note that tumors demonstrate a large degree of random variation in vessel length and diameter, making precise matching more difficult. Tumor blood flow is also highly variable and often consists of leaky irregular sinuses with incomplete basement membranes. Moreover, in a clinical setting, large hepatocellular carcinomas may be accompanied by intratumoral arterioportal or arteriovenous

NIH-PA Author Manuscript

NIH-PA Author Manuscript

NIH-PA Author Manuscript

shunts, and caution should be paid when choosing the smaller size of embolic particles. Such aspects of the tumor microenvironment must be considered when choosing microspheres based on size for penetration inside tumors.

The present study has several limitations. The embolic and/or tumoricidal effects of these microspheres were not studied. Further investigations should be performed to demonstrate whether the increased distal arterial embolization provided by the use of the smaller IOEs allows greater tumor kill. Long-term MR imaging follow-up and histopathologic analysis was also not performed, as the study is focused on microsphere detectability and preferential distribution. In this study, we also chose not to calculate liver iron concentration or estimate hepatic iron content with proton transverse relaxation rate R2 images, as our aim was to qualitatively and not quantitatively analyze the IOE distribution.

In summary, we found that iron-loaded tris-acryl gelatin microspheres could easily be tracked by MR imaging, allowing immediate determination of the distribution of the microspheres in the liver. We also found that the distribution of these microspheres differed greatly according to their respective size. The smaller microspheres (100–300 μm) were found delivered within the tumor itself or, at the very minimum, within the rim of the tumor, whereas the 300–500-μm microspheres clustered within the hepatic artery outside the tumor. This preferential distribution may have important clinical implications, especially regarding drug delivery with use of drug-eluting microspheres.

Abbreviation

IOE, iron oxide– containing Embosphere.

Acknowledgment

The authors thank Philippe Reb, PhD, from Biosphere Medical, for his help regarding the in vitro testing of IOEs.

This research was funded in part by grants from Genentech (South San Francisco, California), MDS Nordion (Ottawa, Ontario, Canada), Biocompatibles (Surrey, United Kingdom), Biosphere Medical (Rockland, Massachusetts), Boston Scientific Oncology (Natick, Massachusetts), and The Charles W. Pratt Foundation for Liver Cancer. K.H.L. is a salaried employee of Boston Scientific. J.F.H.G. serves as a paid consultant for MDS Nordion, Biocompatibles, Biosphere Medical, Terumo (Tokyo, Japan), and Boston Scientific.

References

1. Lau WY, Ho S, Leung TWT, et al. Selective internal radiation therapy for nonresectable hepatocellular carcinoma with intraarterial infusion of 90yttrium microspheres. Int J Radiat Oncol Biol Phys 1998;40:583–592. [PubMed: 9486608]
2. Stuart K. Chemoembolization in the management of liver tumors. Oncologist 2003;8:425–437. [PubMed: 14530495]
3. Liapi E, Geschwind JFH. Transcatheter and ablative therapeutic approaches for solid malignancies. J Clin Oncol 2007;25:978–986. [PubMed: 17350947]
4. Maluccio M, Covey AM, Gandhi R, et al. Comparison of survival rates after bland arterial embolization and ablation versus surgical resection for treating solitary hepatocellular carcinoma up to 7 cm. J Vasc Interv Radiol 2005;16:955–961. [PubMed: 16002503]
5. Okada H, Toguchi H. Biodegradable microspheres in drug-delivery. Crit Rev Ther Drug Carrier Syst 1995;12:1–99. [PubMed: 8521523]
6. Davis SS. Biomedical applications of nanotechnology - implications for drug targeting and gene therapy. Trends Biotechnol 1997;15:217–224. [PubMed: 9183864]
7. Laurent A, Beaujeux R, Wassef M, Rufenacht D, Boschetti E, Merland JJ. Trisacryl gelatin microspheres for therapeutic embolization, I: development and in vitro evaluation. AJNR Am J Neuroradiol 1996;17:533–540. [PubMed: 8881250]

NIH-PA Author Manuscript

NIH-PA Author Manuscript

NIH-PA Author Manuscript

8. Lewis A, Gonzalez M, Leppard S, et al. Doxorubicin eluting beads – 1: effects of drug loading on bead characteristics and drug distribution. J Mater Sci Mater Med 2007;18:1691–1699. [PubMed: 17483878]
9. Gonzalez M, Tang Y, Phillips G, et al. Doxorubicin eluting beads—2: methods for evaluating drug elution and in-vitro:in-vivo correlation. J Mater Sci Mater Med 2008;19:767–775. [PubMed: 17653626]
10. Vallee JN, Lo D, Guillevin R, Reb P, Adem C, Chiras J. In vitro study of the compatibility of tris-acryl gelatin microspheres with various chemotherapeutic agents. J Vasc Interv Radiol 2003;14:621–628. [PubMed: 12761316]
11. Josephson L, Lewis J, Jacobs P, Hahn PF, Stark DD. The effects of iron oxides on proton relaxivity. Magn Reson Imaging 1988;6:647–653. [PubMed: 2850434]
12. Lee HS, Hee Kim E, Shao H, Kook Kwak B. Synthesis of SPIO-chitosan microspheres for MRI-detectable embolotherapy. J Magnet Magn Mater 2005;293:102–105.
13. Pardoe H, Clark PR, St. Pierre TG, Moroz P, Jones SK. A magnetic resonance imaging based method for measurement of tissue iron concentration in liver arterially embolized with ferromagnetic particles designed for magnetic hyperthermia treatment of tumors. Magn Reson Imaging 2003;21:483–488. [PubMed: 12878257]
14. Moroz P, Jones SK, Winter J, Gray BN. Targeting liver tumors with hyperthermia: ferromagnetic embolization in a rabbit liver tumor model. J Surg Oncol 2001;78:22–29. [PubMed: 11519064]
15. Pillai KM, McKeever PE, Knutsen CA, Terrio PA, Prieskorn DM, Ensminger WD. Microscopic analysis of arterial microsphere distribution in rabbit liver and hepatic VX2 tumor. Sel Cancer Ther 1991;7:39–48. [PubMed: 1754728]
16. Stampfl S, Stampfl U, Rehnitz C, et al. Experimental evaluation of early and long-term effects of microparticle embolization in two different mini-pig models. Part II: liver. Cardiovasc Intervent Radiol 2007;30:462–428. [PubMed: 17342551]
17. Yamamoto A, Imai S, Kobatake M, Yamashita T, Tamada T, Umetani K. Evaluation of tris-acryl gelatin microsphere embolization with monochromatic x rays: comparison with polyvinyl alcohol particles. J Vasc Interv Radiol 2006;17:1797–1802. [PubMed: 17142710]
18. Hong K, Khwaja A, Liapi E, Torbenson MS, Georgiades CS, Geschwind JF. New intra-arterial drug delivery system for the treatment of liver cancer: preclinical assessment in a rabbit model of liver cancer. Clin Cancer Res 2006;12:2563–2567. [PubMed: 16638866]
19. Hong K, Kobeiter H, Georgiades CS, Torbenson MS, Geschwind JFH. Effects of the type of embolization particles on carboplatin concentration in liver tumors after transcatheter arterial chemoembolization in a rabbit model of liver cancer. J Vasc Interv Radiol 2005;16:1711–1717. [PubMed: 16371540]
20. Namur J, Chapot R, Pelage JP, et al. MR imaging detection of superparamagnetic iron oxide loaded tris-acryl embolization microspheres. J Vasc Interv Radiol 2007;18:1287–1295. [PubMed: 17911520]
21. Moroz P, Metcalf C, Gray BN. Histologic analysis of liver tissue following hepatic arterial infusion of ferromagnetic particles in a rabbit tumour model. Biometals 2003;16:455–464. [PubMed: 12680709]
22. Laurent A, Wassef M, Chapot R, Houdart E, Merland JJ. Location of vessel occlusion of calibrated tris-acryl gelatin microspheres for tumor and arteriovenous malformation embolization. J Vasc Interv Radiol 2004;15:491–496. [PubMed: 15126660]
23. Majumdar S, Zoghbi S, Pope CF, Gore JC. A quantitative study of relaxation rate enhancement produced by iron oxide particles in polyacrylamide gels and tissue. Magn Reson Med 1989;9:185–202. [PubMed: 2716504]

NIH-PA Author Manuscript
NIH-PA Author Manuscript
NIH-PA Author Manuscript

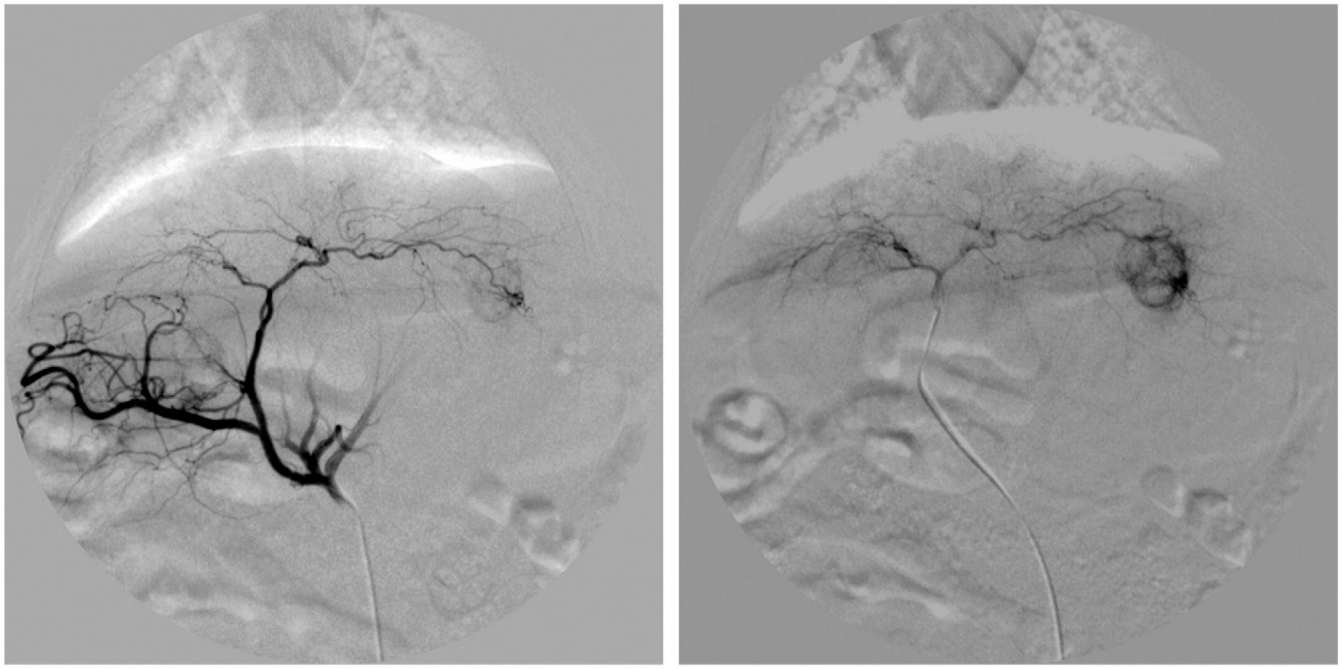

a. b.

Figure 1.

Hepatic artery digital subtraction angiography in a rabbit. **(a)** Digital subtraction angiographic image of the celiac axis demonstrates typical rabbit hepatic arterial anatomy. The VX2 tumor stain is visible within the left lateral lobe of the liver. **(b)** On digital subtraction angiographic image at the proper hepatic artery before treatment, note the intense tumor blush within the left lateral lobe of the liver.

NIH-PA Author Manuscript
NIH-PA Author Manuscript
NIH-PA Author Manuscript

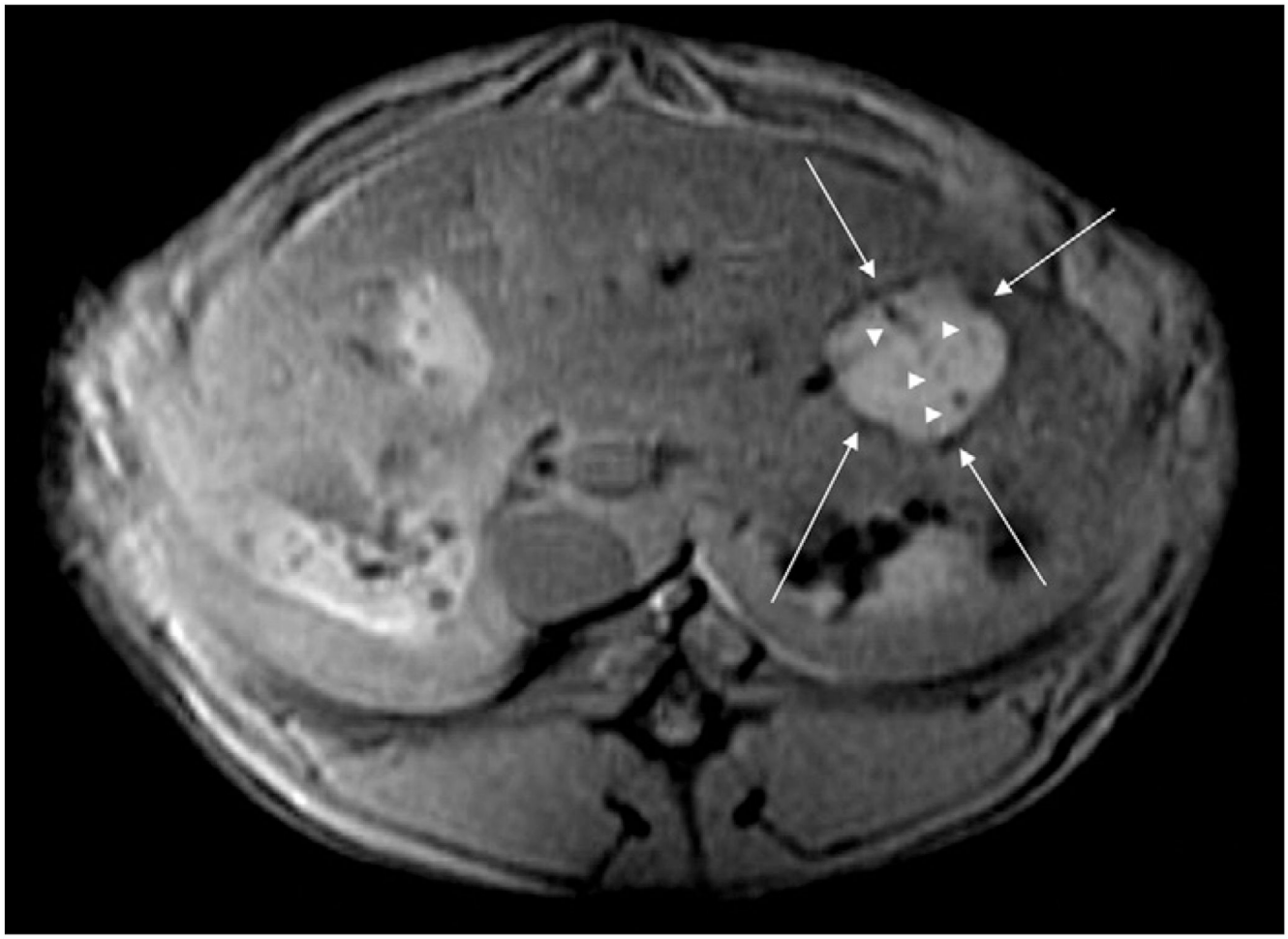

Figure 2.
Axial T2*-weighted MR image (field of view, 16 × 16; matrix size, 256 × 160; repetition/echo time, 200/15 msec; flip angle, 45°) of the liver after embolization with 100–300-μm IOEs. Note the multiple punctate signal voids inside the tumor (arrowheads) and circumferentially distributed at the rim of the tumor (white arrows), showing the ability of MR imaging to track the distribution of IOEs in tumor bed.

NIH-PA Author Manuscript

NIH-PA Author Manuscript

NIH-PA Author Manuscript

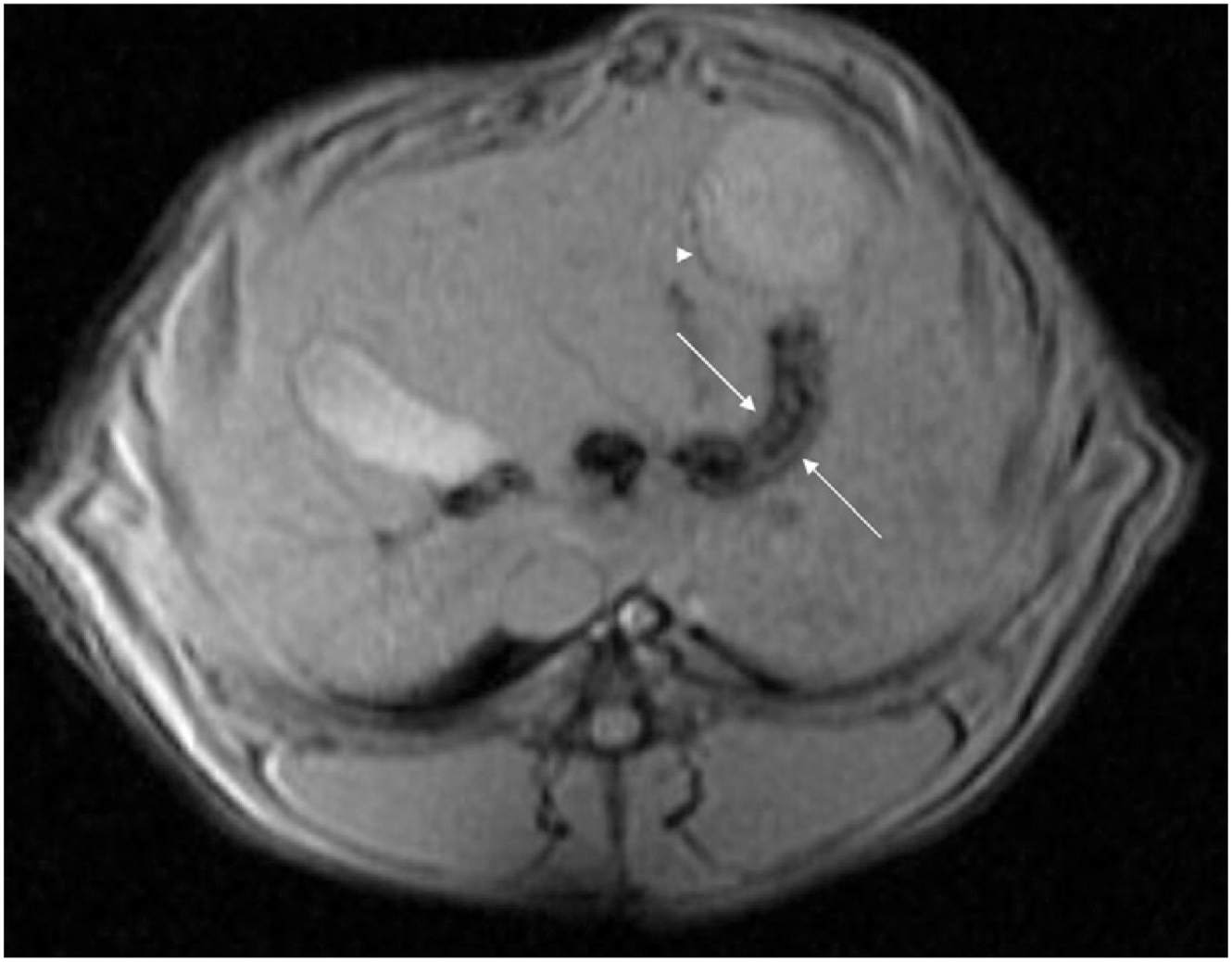

Figure 3.
Axial T2*-weighted MR image of the liver after embolization with 300–500-μm IOEs. Less intense and partially distributed signal void at the rim of the tumor (arrowhead) is seen without signal void inside the tumor. Note the intense signal void with blooming artifact (white arrow) caused by the clustered IOEs within the left hepatic artery located at a significant distance from the tumor bed.

NIH-PA Author Manuscript

NIH-PA Author Manuscript

NIH-PA Author Manuscript

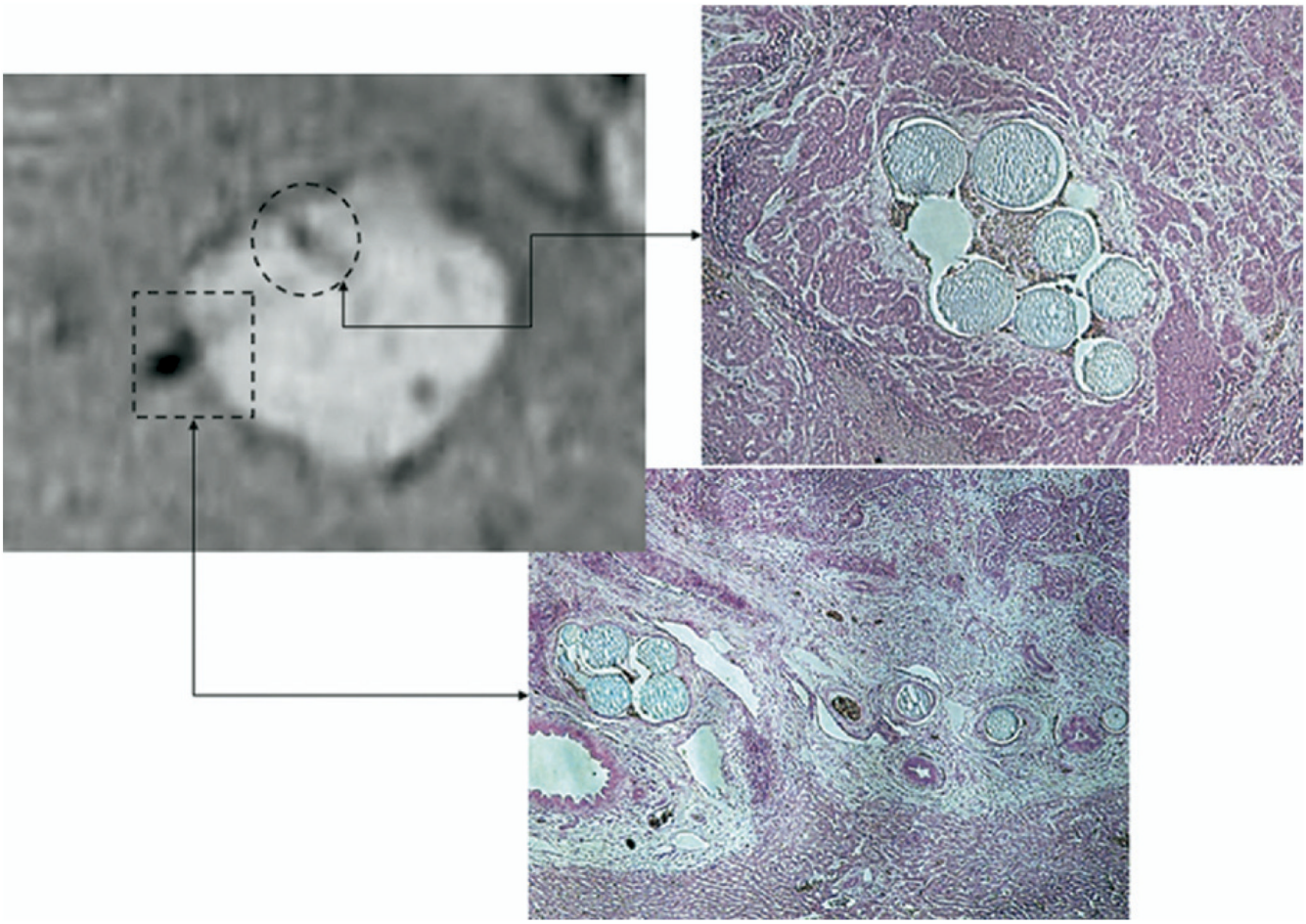

Figure 4.
MR Imaging and histopathologic correlation in an animal in group S treated with 100–300-μm IOEs. Good deposition of particles in the tumor bed at the intracapsular deposition of periphery of the tumor and inside the tumor. Prussian blue staining demonstrates iron-loaded blue-colored embolic materials.

NIH-PA Author Manuscript

NIH-PA Author Manuscript

NIH-PA Author Manuscript

Quantification of IOE Distribution According to Size

Finding	Group SM (100 –300-μm IOE)	Group L (300 –500-μm IOE)	*P* Value
MR Imaging			
MR sensitivity	10/10 (100)	10/10 (100)	
Quantification score	20	16	<.05
Artifact in artery	10/10 (100)	10/10 (100)	
Artifact in tumor bed			<.05
Periphery of tumor	10/10 (100)	6/10 (60)	
Inside tumor	3/10 (30)	0/10	
Histopathology			
Quantification score	20	14	<.05
IOEs in artery	10/10 (100)	10/10 (100)	
IOEs in tumor bed			<.05
Periphery of tumor	10/10 (100)	4/10 (40)	
Inside tumor	7/10 (70)	0/10	

Note.—Values in parentheses are percentages.